University of Groningen

Bilayer-Ternary Polymer Solar Cells Fabricated Using Spontaneous Spreading on Water

Colberts, Fallon J. M.; Wienk, Martijn M.; Heuvel, Ruurd; Li, Weiwei; Le Corre, Vincent M.; Koster, L. Jan Anton; Janssen, Rene A. J.

IMPORTANT NOTE: You are advised to consult the publisher's version (publisher's PDF) if you wish to cite from it. Please check the document version below.

Document Version
Publisher's PDF, also known as Version of record

Link to publication in University of Groningen/UMCG research database

Bilayer–Ternary Polymer Solar Cells Fabricated Using Spontaneous Spreading on Water

Fallon J. M. Colberts, Martijn M. Wienk, Ruurd Heuvel, Weiwei Li, Vincent M. Le Corre, L. Jan Anton Koster, and René A. J. Janssen*

A new method is presented to fabricate bilayer organic solar cells via sequential deposition of bulk-heterojunction layers obtained using spontaneous spreading of polymer–fullerene blends on a water surface. Using two layers of a small bandgap diketopyrrolopyrrole polymer–fullerene blend, a small improvement in power conversion efficiency (PCE) from 4.9% to 5.1% is obtained compared to spin-coated devices of similar thickness. Next, bilayer–ternary cells are fabricated by first spin coating a wide bandgap thiophene polymer–fullerene blend, followed by depositing a small bandgap diketopyrrolopyrrole polymer–fullerene layer by transfer from a water surface. These novel bilayer–ternary devices feature a PCE of 5.9%, higher than that of the individual layers. Remarkable, external quantum efficiencies (EQEs) over 100% are measured for the wide bandgap layer under near-infrared bias light illumination. Drift-diffusion calculations confirm that near-infrared bias illumination can result in a significant increase in EQE as a result of a change in the internal electric field in the device, but cannot yet account for the magnitude of the effect. The experimental results indicate that the high EQEs over 100% under bias illumination are related to a barrier for electron transport over the interface between the two blends.

1. Introduction

Due to the advantages of solution processing, flexibility, high throughput production, and color tunability, organic photovoltaics (OPVs) have been receiving wide interest.[1,2] Improving the power conversion efficiency (PCE) of these devices has been the focus point of research resulting in a gradual increasing performance above 10% based on mixtures of semiconducting polymers with fullerene derivatives.[3–6] Because fullerenes have limited structural tunability and weak absorption in the visible region, nonfullerene acceptors are attracting pronounced attention recently to further enhance the efficiency,[7–10] resulting in PCEs up to 14%.[11–14] An interesting strategy to broaden the absorption spectra of organic solar cells is to blend multiple donor (D) or acceptor (A) materials into one bulk heterojunction resulting in D_1:D_2:A or D:A_1:A_2 blends. Ternary blend cells have several advantages such as enhanced spectral coverage due to the complementary absorption of the three components, improved fill factor (FF) by morphology optimization, and optimized device stability.[15,16] The latter can be specifically achieved by D:A_1:A_2 blends in which the acceptor mixture forms an alloy phase. The glassy property of this phase increases the entropy of mixing for the two acceptors and reduces the rate of crystallization.[15,17] Results on D_1:D_2:A blends showed that the addition of a crystalline polymer to an amorphous host can improve charge separation and transport in the device, improving its FF. This is facilitated by charge transfer from a trap-limited disordered phase to a highly ordered phase having a high mobility.[18,19] Reported efficiencies above 10% indicate that ternary blends are a promising strategy in overcoming some of the limitations of polymer solar cells without complicating the processing procedure.[20–22] However, the introduction of a third component does complicate the understanding and control on the layer morphology

F. J. M. Colberts, Dr. M. M. Wienk, Dr. R. Heuvel, Prof. R. A. J. Janssen
Molecular Materials and Nanosystems
Institute for Complex Molecular Systems
Eindhoven University of Technology
P. O. Box 513, 5600 MB, Eindhoven, The Netherlands
E-mail: r.a.j.janssen@tue.nl

The ORCID identification number(s) for the author(s) of this article can be found under https://doi.org/10.1002/aenm.201802197.

Prof. W. Li
Beijing National Laboratory for Molecular Sciences
Key Laboratory of Organic Solids
Institute of Chemistry
Chinese Academy of Sciences
Beijing 100190, P. R. China
V. M. Le Corre, Prof. L. J. A. Koster
Photophysics and Optoelectronics
Zernike Institute for Advanced Materials
University of Groningen
Nijenborgh 4, 9747 AG Groningen, The Netherlands
Prof. R. A. J. Janssen
Dutch Institute for Fundamental Energy Research
De Zaale 20, 5612 AJ Eindhoven, The Netherlands

ADVANCED
SCIENCE NEWS
www.advancedsciencenews.com

ADVANCED
ENERGY
MATERIALS
www.advenergymat.de

and charge transport through the device. Domain purity, size, and crystallinity are critical parameters determining the device performance which are nowadays well controlled in binary bulk heterojunctions, but this knowledge is less well developed for ternary devices.[19,23,24] Additionally, the majority of ternary devices reported are restrained to ≈20% incorporation of a third component, because at higher concentrations, the FF and short-circuit current density (J_{SC}) decrease.[19,20,25–27] This limits PCE improvement with respect to the performance of the corresponding binary devices.

Fabricating D_1:A|D_2:A bilayer–ternary photovoltaics by processing two binary blends on top of each other would allow the use of conventional well-developed, high-performance active layers. These bilayer–ternary configurations are rarely reported as they are challenging to fabricate by solution coating methods, because the underlying layer is likely to dissolve when the second layer is processed on top. Ghasemi et al. developed a method which does not require orthogonal solvents for the processing of bilayer–ternary devices. Both D_1:A and D_2:A blends are processed on top of each other from the same solvent, taking advantage of the low solubility of D_1 at room temperature, the first layer was spin-coated hot (without cosolvents) and the D_2:A blend could be processed on top at room temperature.[28] Although the current density of the device improved significantly, the performance of the ternary

device suffered from a low FF due to increased active layer thickness, limiting the performance improvement of the ternary device compared to the best performing binary blend. The required robustness of the first layer restrains the generality of this method. Another method to fabricate bilayer architectures for organic active layers is by lamination. Here, the two active layers are fabricated separately of which one layer is processed on a polyurethane acrylate (PUA)-coated substrate. This "mold" is stamped on top of the second blend, while the layer detaches from the PUA coating.[29,30]

Noh et al. recently demonstrated that spontaneous spreading on a water substrate, schematically depicted in **Figure 1**, in combination with transfer to a secondary substrate allows processing of multiple active layers on top of each other, resulting in efficient solar cells.[31] In this method, a droplet of a solution containing the photoactive materials is dropped on a water substrate and spreads due to surface tension differences (Marangoni flow). Whether the solution spreads or forms a lens on the water surface, is determined by the spreading coefficient

$$S_{ow} = \gamma_{w(o)} - \gamma_{o(w)} - \gamma_{ow} \qquad (1)$$

where S_{ow} is the spreading coefficient of the organic liquid on a water surface, $\gamma_{w(o)}$ is the surface tension of water saturated with the organic liquid, $\gamma_{o(w)}$ is the surface tension of the
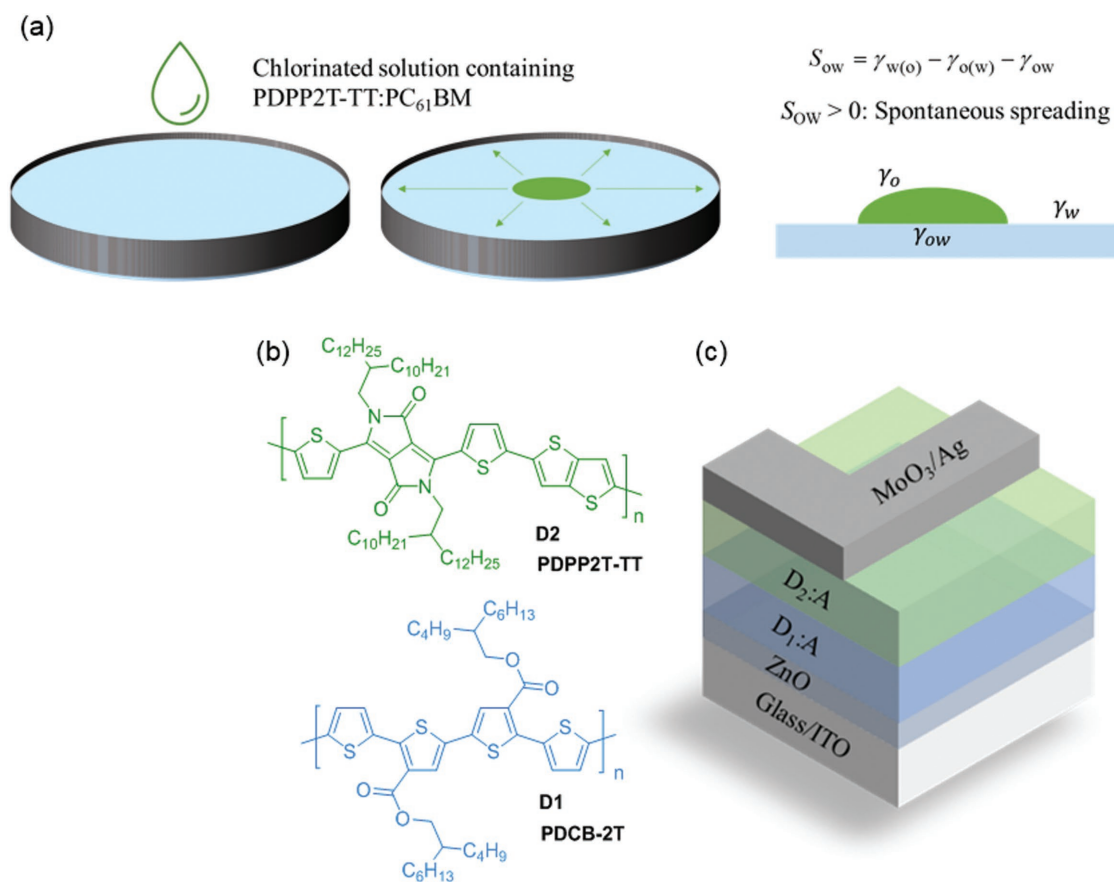

Figure 1. a) Schematic of the spontaneous spreading technique. b) Chemical structures of the small bandgap PDPP2T-TT (D_2) and wide bandgap PDCB-2T (D_1) polymers. c) Inverted device architecture of the bilayer–ternary cell.

ADVANCED
SCIENCE NEWS
www.advancedsciencenews.com

ADVANCED
ENERGY
MATERIALS
www.advenergymat.de

organic liquid saturated with water, and γ_{ow} is the interfacial tension between water and the organic liquid.[32] The latter reflects the difference between intermolecular forces within the bulk liquid and the intermolecular forces between the liquids. When the surface tension of the organic solvent is not too high, the spreading coefficient will be positive, meaning that the liquid will spread. However, when the coefficient is negative, it will form a lens.[33] The former is the case for both chloroform ($S_{ow} = 72.6 - 27.3 - 32.8 = 12.4$ mN m^{-1}) and chlorobenzene ($S_{ow} = 71.6 - 33.6 - 37.4 = 0.6$ mN m^{-1}).[32] Noh et al. reported that layers of poly[[4,8-bis[(2-ethylhexyl)oxy]benzo[1,2-*b*:4,5-*b'*]dithiophene-2,6-diyl][3-fluoro-2-[(2-ethylhexyl)carbonyl]-thieno[3,4-*b*]thiophenediyl]] (PTB7) mixed with [6,6]-phenyl-C$_{71}$-butyric acid methyl ester (PC$_{71}$BM) from chlorobenzene can be made by this method with a comparable PCE in a device as spin-coated layers. The method takes its advantage in the ability to process PTB7:PC$_{71}$BM devices under ambient conditions while spin coating requires an inert environment. Furthermore, the method can easily be transformed into a large-scale production process.[31]

In this work, the spontaneous spreading technique has been used for multilayer stacking which allows the fabrication of novel bilayer–ternary device architectures. For this purpose, layers composed of PC$_{61}$BM mixed with a small bandgap diketopyrrolopyrrole (DPP) polymer (PDPP2T-TT) in which the DPP unit is flanked by two thiophene units (2T), polymerized with thienothiophene (TT) (Figure 1) are spread on a water surface. Li et al. showed that due to the high charge carrier mobility originating from the crystalline fiber–like structure of the polymer, a good PCE with high FF can be achieved with thick active layers above 200 nm.[34] This property is of great interest for processing multiple layers on top of each other with the spontaneous spreading method. By transferring twice the same floating active layer on water to a ZnO-coated glass/indium tin oxide (ITO) substrate and subsequent solvent vapor annealing, we fabricate solar cell devices with similar PCEs as those obtained via spin coating (5.1% vs 4.9%). To fabricate bilayer–ternary devices, a wide bandgap polymer

(PDCB-2T) consisting of thiophene-flanked (2,2′-bithiophene)-4,4′-dicarboxylate (DCB) units (Figure 1)[35] was spin-coated with PC$_{61}$BM on a glass/ITO/ZnO substrate on top of which the PDPP2T-TT:PC$_{61}$BM layer is transferred by the spontaneous spreading method. The inverted device architecture of the resulting bilayer–ternary device is shown in Figure 1b. These novel bilayer–ternary devices have a PCE of 5.9%, higher than that of the individual layers. Surprisingly, the cells provide external quantum efficiencies (EQEs) over 100% for the wide bandgap layer under simultaneous near-infrared (NIR) bias light illumination.

2. Results and Discussion

2.1. Solar Cells by Spontaneous Spreading

For the spontaneous spreading method, PDPP2T-TT and PC$_{61}$BM were dissolved in a 1:3 ratio in chlorobenzene containing 10 vol% 1,8-diiodooctane (DIO). Due to its low vapor pressure, DIO does not fully evaporate which gives flexibility and prevents cracking of the spread layer during transfer. The optimization of the solvent mixture is discussed in detail in Section S1 (Supporting Information). Complete dissolution is important to achieve high device performance. 20 µL of this solution is used to cover a Petri dish of 9 cm in diameter filled with water. After two separate depositions of the solution on a water substrate, the two resulting layers are sequentially transferred on top of each other using a glass/ITO/ZnO substrate. The device is completed with a MoO$_3$/Ag top contact. For good performance, it is essential to treat the stack of two PDPP2T-TT:PC$_{61}$BM layers with chloroform vapor for 1 min. The *J–V* characteristics (**Figure 2**a and **Table 1**) show that without this solvent vapor annealing (SVA), the device suffers from charge extraction problems. SVA results in reduced bimolecular recombination, indicated by the light intensity dependent EQE plotted in Figure 2b.[36] Bimolecular recombination in the device results in drop of EQE when the light
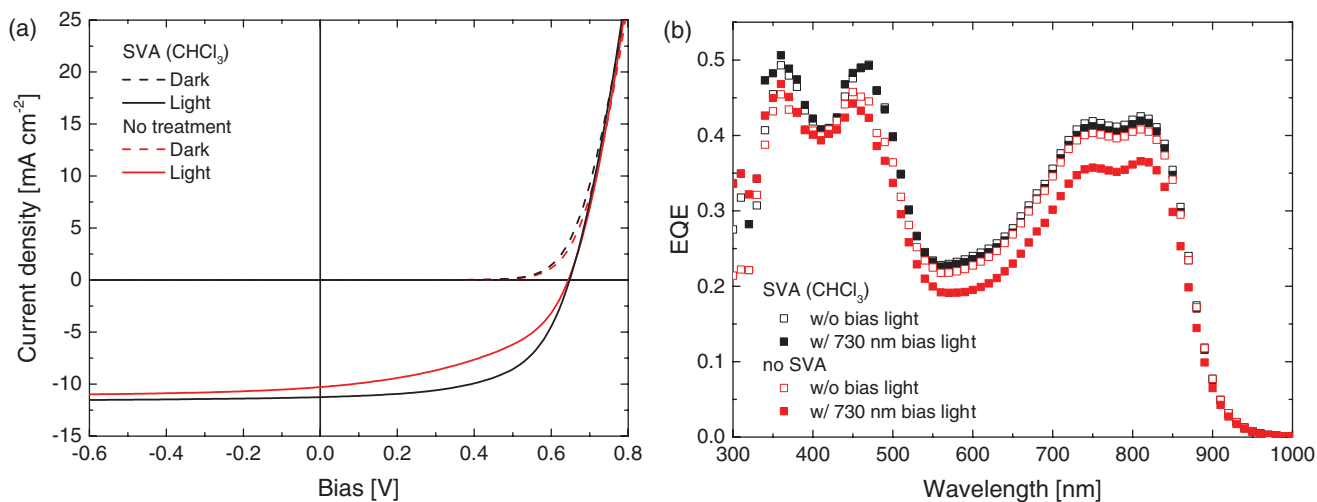
Figure 2. a) *J–V* characteristics of bilayer PDPP2T-TT:PC$_{61}$BM devices fabricated by spontaneous spreading without (red lines) and after solvent (CHCl$_3$) vapor annealing (1 min) (black lines) in dark (dashed lines) and under simulated AM1.5 G illumination (solid lines). b) The corresponding EQE spectra measured without (open makers) or with (solid markers) bias illumination to bring the cells close to AM1.5G operating conditions.

1802197 (3 of 12)

ADVANCED
SCIENCE NEWS
www.advancedsciencenews.com

ADVANCED
ENERGY
MATERIALS
www.advenergymat.de

Table 1. Effect of SVA on the device performance of bilayer PDPP2T-TT:PC$_{61}$BM devices fabricated by the spontaneous spreading method.

Treatment	d [nm]	J_{SC}^{EQE} [mA cm^{-2}][a]	V_{OC} [V][a]	FF[a]	PCE [%][a]
No	189	9.95 (10.1 ± 0.86)	0.64 (0.64 ± 0.00)	0.48 (0.45 ± 0.05)	3.1 (2.9 ± 0.20)
SVA (CHCl$_3$)	154	11.4 (11.2 ± 0.15)	0.65 (0.65 ± 0.00)	0.59 (0.59 ± 0.01)	4.4 (4.3 ± 0.04)

[a]Performance of the best device corrected for J_{SC}^{EQE} and between brackets, the average result ± standard deviation obtained from J–V measurements of 3 devices.

intensity increases. Hence, the ratio (ρ) between the short-circuit currents obtained by integrating the AM1.5G spectrum with the EQE measured with and without bias light illumination ($\rho = J_{SC}^{EQE}$(bias)/J_{SC}^{EQE}(no bias)), serves as a measure of the extent of bimolecular recombination. Without SVA, ρ equals 0.90, while ρ is 0.99 after SVA. This indicates reduced recombination and enhanced charge extraction after SVA. Transmission electron microscopy (TEM) did not reveal a change in domain size upon SVA (Section S2, Supporting Information).

Compared to spin-coated (SC) devices, the performance of spontaneous spreading (SS) devices is somewhat higher (**Table 2**). This is caused by an increased J_{SC} for the SS devices, accompanied by a lower FF. The increased J_{SC} but reduced FF of the bilayer device can be rationalized by a morphological difference observed by TEM (**Figure 3**) (atomic force microscopy (AFM) results are shown in Section S3 in the Supporting Information). Both the active layers have a similar fibrous structure which is known to consist of semicrystalline polymer chains with a preferred stacking in the face-on direction and reduced π–π stacking distance with the application of a cosolvent.[37] Figure 3, however, shows that the width and domain size of the polymer fibers is smaller upon spontaneous spreading of the active layer compared to the spin coating. This results in more donor–acceptor interface and, hence, increased photocurrent generation, but the more tortuous morphology can hamper charge transport and increase charge recombination, resulting in a lower FF. Hence, the change in morphology is consistent with the rise of J_{SC} and the reduction in FF (Table 2). Alternatively, the low FF may be associated with less good Ohmic contacts. In Section S4 (Supporting Information), we show that the performance of devices made by spontaneous spreading is virtually identical for single and bilayer devices at the same total thickness. Hence, the bilayer architecture itself does not result in reduction of the FF seen in Table 2. Moreover, for thinner films ($\approx$130 nm) made by spontaneous spreading, the FF is high (0.66–0.69), as shown in Section S4 (Supporting Information). These results suggest that the contacts are not

limiting but that the morphology is the most likely cause for the reduced FF upon spontaneous spreading of thick bulk heterojunction layers.

2.2. Bilayer–Ternary Solar Cells

The above results demonstrate that the spontaneous spreading method allows processing of multiple active layers on top of each other without efficiency loss. Interestingly, this enables processing of more complicated device architectures like bilayer–ternary solar cells. The first layer of these devices is deposited by spin coating on a ZnO-coated glass/ITO substrate. This solution in chloroform contains the wide bandgap polymer PDCB-2T (Figure 1) in combination with PC$_{61}$BM. Spin-coated PDCB-2T:PC$_{71}$BM layers resulted in a performance of 5% (J_{SC} = 9.66 mA cm^{-2}, V_{OC} = 0.74 V, FF = 0.71).[35] On top of the PDCB-2T:PC$_{61}$BM layer, the PDPP2T-TT:PC$_{61}$BM layer can be deposited via spontaneous spreading on water and subsequent transfer. The energy diagram of the bilayer–ternary device, of which the highest occupied molecular orbital (HOMO) and lowest unoccupied molecular orbital (LUMO) levels are determined by cyclic voltammetry (CV), is illustrated in **Figure 4**a. The two complementary absorption spectra of the D$_1$:A and D$_2$:A layers are shown in Figure 4b. The HOMO levels of the PDPP2T-TT (+0.39 V vs Fc/Fc$^+$) and PDCB-2T (+0.32 V vs Fc/Fc$^+$) are very close in energy, but their optical bandgaps differ considerably (E_g = 1.91 eV vs E_g = 1.35 eV). Hence, the energy levels of photogenerated holes and electrons in the bilayer–ternary blends with PC$_{61}$BM as a common acceptor are fairly constant through the bilayer (Figure 4a).

Table 3 shows that the bilayer–ternary device slightly benefits from the complementary absorption resulting in an enhanced J_{SC} for the best bilayer–ternary device of 5.9% (J–V and EQE of the best performing device are shown in Section S5 in the Supporting Information). However, the statistical data reveal that the variation in J_{SC} is quite large. This is mainly caused

Table 2. Performance of devices fabricated by spontaneous spreading (SS) and spin coating (SC) having similar thicknesses.

Device	d [nm]	J_{SC}^{EQE} [mA cm^{-2}][a]	V_{OC} [V][a]	FF[a]	PCE [%][a]
SS 50/50 CF/CB[b]	216	13.1 (11.9 ± 0.47)	0.67 (0.67 ± 0.00)	0.59 (0.59 ± 0.01)	5.2 (4.7 ± 0.12)
SC	211	10.4 (9.4 ± 0.18)	0.65 (0.65 ± 0.00)	0.67 (0.66 ± 0.02)	4.5 (4.0 ± 0.10)
SS 0/100 CF/CB	287	13.9 (14.3 ± 0.29)	0.67 (0.66 ± 0.00)	0.55 (0.51 ± 0.05)	5.1 (4.8 ± 0.38)
SC	275	11.5 (10.5 ± 0.15)	0.65 (0.62 ± 0.04)	0.67 (0.63 ± 0.04)	4.9 (4.2 ± 0.49)

[a]Performance of the best device corrected for J_{SC}^{EQE} and between brackets, the average result ± standard deviation obtained from J–V measurements of 3 or 4 devices; [b]To reduce the viscosity of the solution in chlorobenzene, a chloroform (CF):chlorobenzene (CB) 1:1 v/v solvent mixture was used. Additional explanation can be found in Section S1 (Supporting Information).
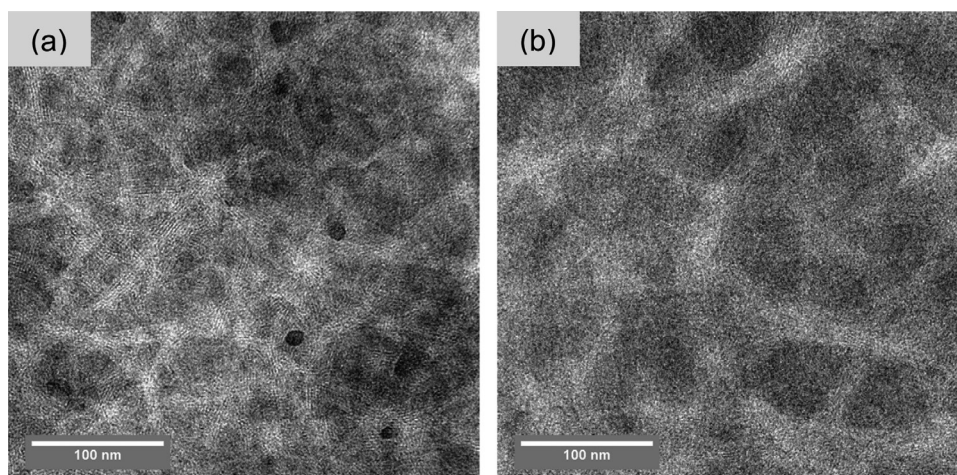
**ADVANCED
SCIENCE NEWS**

www.advancedsciencenews.com

**ADVANCED
ENERGY
MATERIALS**

www.advenergymat.de

Figure 3. a) Active layer morphology of a PDPP2T-TT:PC$_{61}$BM device fabricated by spontaneous spreading from chlorobenzene containing 10 vol% DIO and subsequent SVA treatment. b) Active layer morphology for a device made by spin coating.

by the inhomogeneity of the PDPP2T-TT:PC$_{61}$BM active layers obtained via spontaneous spreading (Section S1, Supporting Information). The average performance of 12 devices having a total thickness between 190 and 210 nm (of which PDCB-2T:PC$_{61}$BM is 100 nm) has PCE = 4.8 ± 0.6% with an average FF of 0.55 and J_{SC} of 12.8 mA cm^{-2}. Compared to a bilayer PDPP2T-TT device with similar active layer thickness, the average FF of the bilayer–ternary cells is somewhat lower (FF = 0.55 vs FF = 0.59 for bilayer–ternary and bilayer PDPP2T-TT devices, respectively). This is reflected in a bias-dependent photocurrent extraction under reverse bias as can be seen in the J–V characteristics of a bilayer–ternary cell (**Figure 5**). From the energy levels of the bilayer–ternary device (Figure 4a), there are no significant barriers for charge extraction, however, illuminating the device with a light-emitting diode (LED) of 530 or 730 nm clearly shows that charges generated in the PDPP2T-TT:PC$_{61}$BM layer are not efficiently collected. Under 730 nm illumination, all photogenerated electrons have to pass the interface between the two bulk heterojunctions and we

suspect that this interface causes the electron extraction problems. As the photon flux of the 730 and 530 nm probe light used for the J–V measurements in Figure 5a is not comparable ($I_{730\,nm} = 3.0 \times 10^{17}$ cm^2 s^{-1} and $I_{530\,nm} = 1.1 \times 10^{17}$ cm^2 s^{-1}), the J_{SC} values cannot be compared directly.

The EQE spectra depicted in Figure 5 clearly show the contribution of PDCB-2T (D$_1$) in the low wavelength regime and of PDPP2T-TT (D$_2$) in the high wavelength regime. It is remarkable that the EQE of the PDPP2T-TT:PC$_{61}$BM layer ($d \approx 100$ nm) in the bilayer–ternary cell is only 25%, while it is above 40% for a single layer ($d \approx 100$ nm) (Figure S5, Supporting Information). This indicates inefficient charge extraction from the PDPP2T-TT:PC$_{61}$BM layer in the bilayer–ternary cell.

More insight into this matter is obtained by measuring the EQE of the cells with bias light of different wavelengths. When using 530 nm bias light, additional charge carriers are predominantly generated in the PDCB-2T:PC$_{61}$BM layer, while with 730 nm bias light, additional charges are exclusively generated in PDPP2T-TT:PC$_{61}$BM. Interestingly, 530 or 730 nm
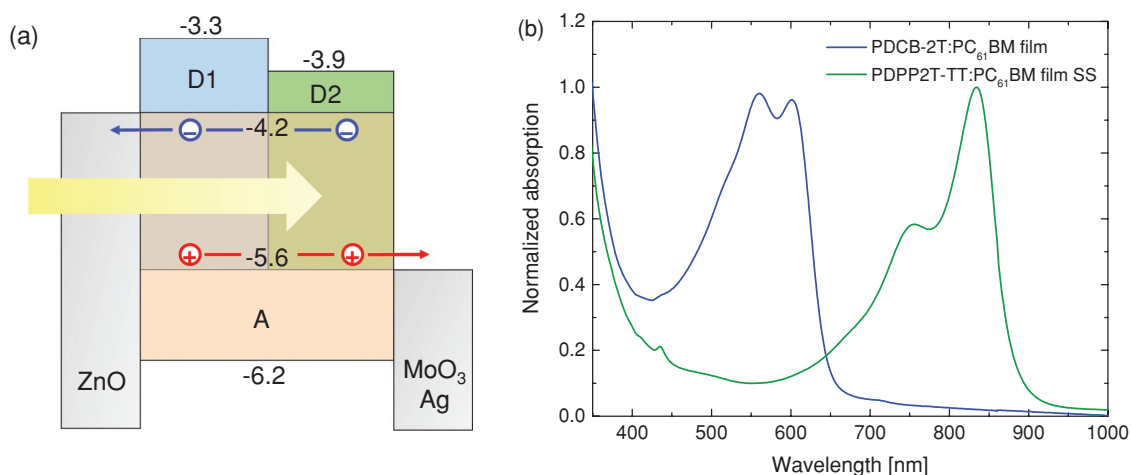

Figure 4. a) Energy diagram indicating the HOMO and LUMO energy levels as determined by CV and device architecture of an inverted bilayer–ternary device. b) Absorption spectra of both the PDCB-2T:PC$_{61}$BM (D$_1$:A) and PDPP2T-TT:PC$_{61}$BM (D$_2$:A) bulk heterojunction layers.

ADVANCED
SCIENCE NEWS
www.advancedsciencenews.com

ADVANCED
ENERGY
MATERIALS
www.advenergymat.de

Table 3. Device performance of the bilayer–ternary solar cells.

Device	d [nm]	J_{SC} [mA cm^{-2}][a]	V_{OC} [V][a]	FF[a]	PCE [%][a]
Bilayer–ternary D$_1$:A | D$_2$:A	203[b]	14.9[c] (12.8 ± 1.4)	0.68 (0.68 ± 0.02)	0.58 (0.55 ± 0.04)	5.9 (4.8 ± 0.6)
Bilayer D$_2$:A | D$_2$:A	216	13.1 (11.9 ± 0.18)	0.67 (0.67 ± 0.00)	0.59 (0.59 ± 0.01)	5.2 (4.7 ± 0.1)
D$_1$:A	100	8.2 (8.0 ± 0.13)	0.69 (0.69 ± 0.00)	0.62 (0.62 ± 0.01)	3.5 (3.4 ± 0.1)

[a]Performance of the best device corrected for J_{SC}^{EQE} and between brackets, the average result ± standard deviation obtained from J–V measurements of 3 or 4 devices; [b]Total active layer thickness of which D$_1$:A is 100 nm; [c]Data point obtained from J–V measurements instead of EQE integration.

bias illumination results in markedly different EQE spectra (Figure 5b). While applying 530 nm bias light, an ≈30% EQE improvement was observed in the high wavelength regime (>650 nm). When applying 730 nm bias light, the EQE more than doubles and increases to values higher than 100%, in the low wavelength regime (<650 nm), while it decreases in the long wavelength range (>650 nm). Apparently, the increased charge density in the PDPP2T-TT:PC$_{61}$BM layer with 730 nm bias illumination enhances recombination, further evidenced by sublinear light intensity–dependent short-circuit current (Figure 5, $\alpha = 0.94$). In contrast, bimolecular recombination in the PDCB-2T:PC$_{61}$BM layer is negligible under short-circuit
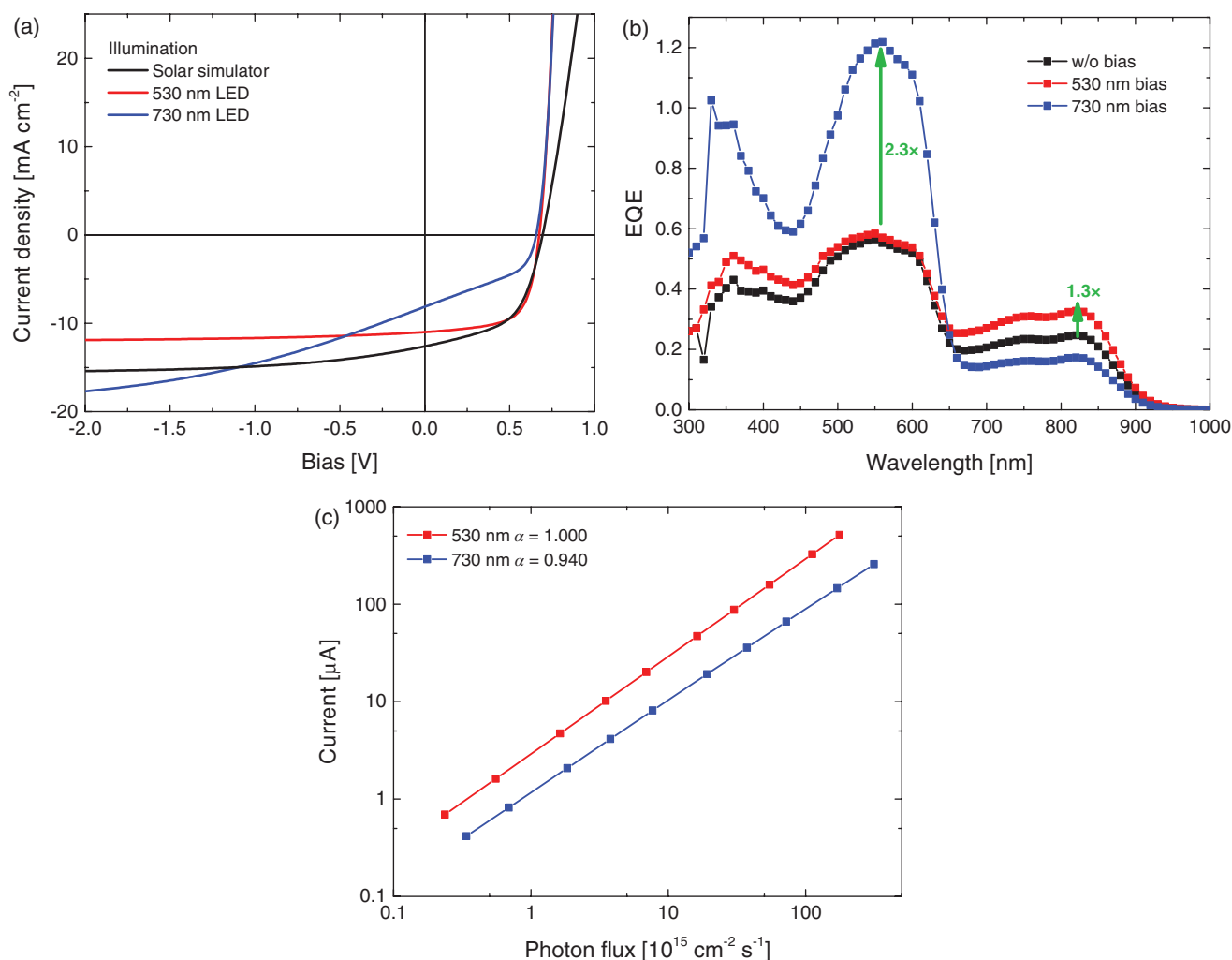

Figure 5. a) J–V characteristics of a bilayer–ternary device in an inverted configuration illuminated with different light sources ($I_{730\,nm} = 3.0 \times 10^{17}$ cm^2 s^{-1} and $I_{530\,nm} = 1.1 \times 10^{17}$ cm^2 s^{-1}). The bilayer–ternary cell consists of a 100 nm PDCB-2T:PC$_{61}$BM bottom layer and 94 nm PDPP2T-TT:PC$_{61}$BM top layer. $J_{SC} = 12.6$ mA cm^{-2}, $V_{OC} = 0.69$ V, FF = 0.54, $P_{max} = 4.7$ mW cm^{-2} with simulated AM1.5G illumination. b) EQE measured without and with 530 or 730 nm bias light. $J_{SC}^{EQE} = 11.2$ mA cm^{-2} (w/o bias light). c) Photocurrent generated by the bilayer device as a function of photon flux and fit of the data to $J_{SC} \propto P_{light}^{\alpha}$.
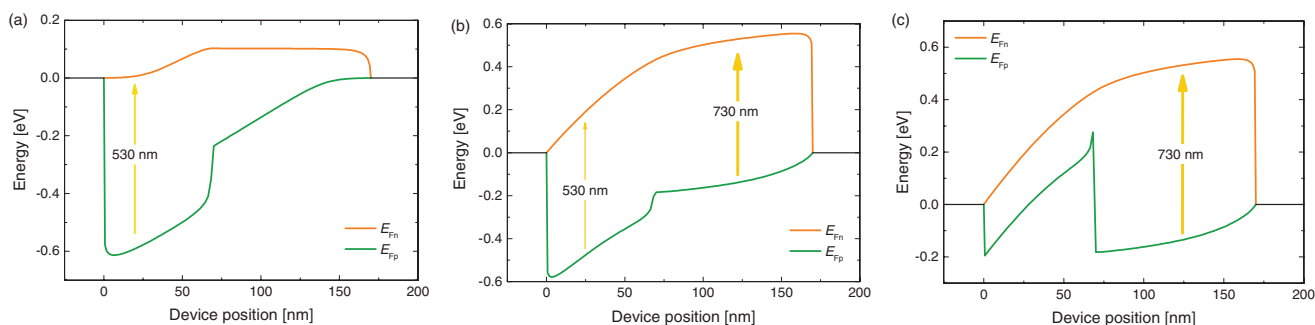
Figure 6. Simulations of the quasi-Fermi levels for electrons (E_{Fn}) and holes (E_{Fp}) by drift-diffusion calculations for bilayer device consisting of 70 nm D_1:A and 100 nm D_2:A under different illumination conditions. a) $G_1 = 10^{26}$ m^{-3} s^{-1}, $G_2 = 0$, representing 530 nm probe light. b) $G_1 = 10^{26}$ m^{-3} s^{-1}, $G_2 = 10^{28}$ m^{-3} s^{-1}, representing 530 nm probe + 730 nm bias light. c) $G_1 = 0$ m^{-3} s^{-1}, $G_2 = 10^{28}$ m^{-3} s^{-1}, representing 730 nm bias illumination.

conditions ($\alpha = 1.00$). These results indicate that the collection of the charges generated in the PDPP2T-TT:PC$_{61}$BM layer of the bilayer–ternary cell is problematic.

Due to the complementary absorption of the two sublayers, charge generation throughout the device is strongly inhomogeneous when illuminated with a bias source resulting in an inhomogeneous electric field. To shed light on these complex changes, drift-diffusion calculations were performed. The details can be found in the Experimental Section. Low intensity ($\approx 10^{15}$ photons cm^2 s^{-1}) 530 nm probe light is mainly absorbed by the PDCB-2T:PC$_{61}$BM (D$_1$:A) layer, resulting in splitting of the quasi-Fermi energy levels, as depicted in **Figure 6**a. Additional absorption of high intensity ($\approx 10^{17}$ photons cm^2 s^{-1}) 730 nm bias light by the PDPP2T-TT:PC$_{61}$BM (D$_2$:A) layer results in an increased quasi-Fermi level splitting in the second layer (D$_2$:A), which concomitantly causes an enhanced electric field over the first layer (D$_1$:A). This leads to improved electron collection efficiency of charges generated by the 530 nm probe light. In the calculations, the EQE at 530 nm is improved by 22%. Although the improvement is significantly less than the experimental result, the result that bias illumination of the second layer can increase the EQE of the first layer is reproduced. The calculations also demonstrate that 530 nm probe light, absorbed by the first layer (D$_1$:A), has no effect on the electric field distribution of the second layer (D$_2$:A) when this is illuminated with 730 nm bias light. In other words, in the calculations, the efficiency of collection of charges generated by 730 nm bias light is not improved by 530 nm probe light. This could have been an explanation for the EQE at 530 nm being higher than 100%. From the drift-diffusion calculations, it thus seems that an enhanced internal electric field induced by 730 nm bias illumination does explain the enhanced EQE but cannot account for the observed magnitude of the effect. Similar calculations have been performed for the situation with 730 nm probe light and 530 nm bias illumination (Section S6, Supporting Information). Also in this situation, 530 nm bias illumination of the first layer (D$_1$:A) results in an increased electric field in the second layer (D$_2$:A), resulting in more efficient collection of holes generated by 730 nm probe light and an improved EQE at 730 nm by 23%. This is in fair agreement with the experimentally average increase in EQE of 30% (Figure 5b).

In our view, an EQE above 100% at 530 nm can only be explained by more efficient collection of 730 nm bias–generated charges when illuminating the device simultaneously with 530 nm monochromatic probe light. **Figure 7** shows that increasing the intensity in the low wavelength regime by
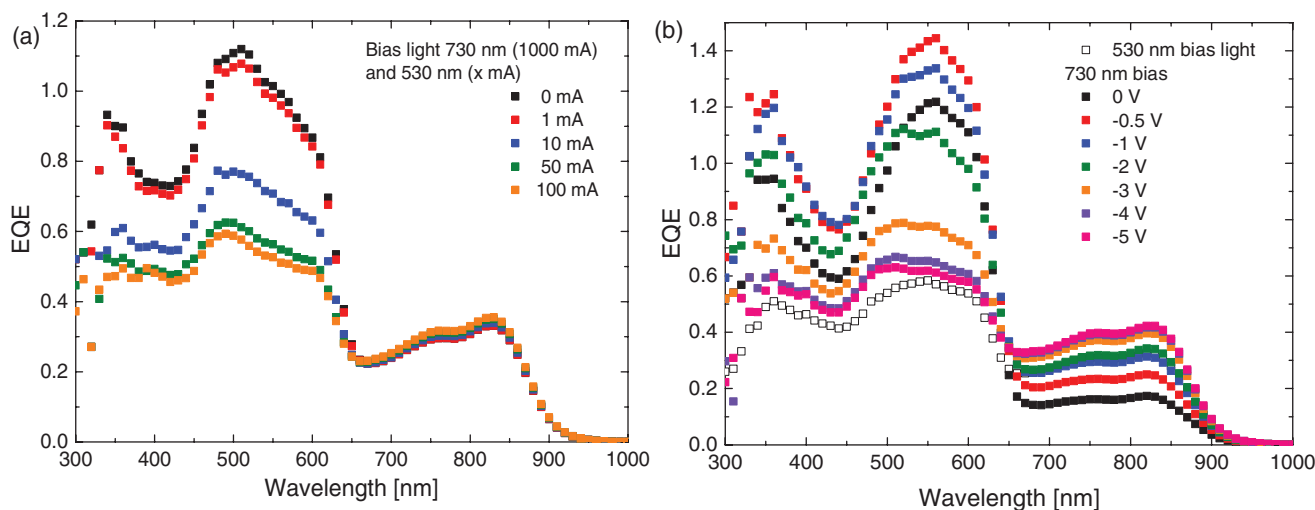

Figure 7. Mitigation of the EQE enhancement by a) increasing the intensity of an additional 530 nm LED source to the 730 nm bias light and monochromatic probe light and b) increased reverse bias.

**ADVANCED
SCIENCE NEWS**
www.advancedsciencenews.com

**ADVANCED
ENERGY
MATERIALS**
www.advenergymat.de

applying a second bias light source at 530 nm, in addition to 730 nm bias and monochromatic probe light, reduces the EQE. Likewise, a decrease of the intensity of the 730 nm bias source (Section S7, Supporting Information) reduces the EQE overshoot. We suggest that an energy barrier is formed at the interface between the two sublayers, hampering electron transport from the PDPP2T-TT:PC$_{61}$BM layer toward the ZnO contact. In a way that is not fully understood, the increased carrier density in the PDCB-2T:PC$_{61}$BM layer lowers this barrier and accumulation of electrons. Apparently, the height of this energy barrier is significant because a high reverse bias is required to eliminate its effect on the EQE measurement with 730 nm bias. Figure 7 shows that a reverse bias of 4–5 V is required to level out the EQE enhancement. This is consistent with the increasing extracted current density with reverse bias by J–V measurements under 730 nm illumination (Figure 5a). In addition, the reverse bias increases the EQE of the PDPP2T-TT:PC$_{61}$BM layer to a similar value compared to a PDPP2T-TT:PC$_{61}$BM-only device (Figure S5, Supporting Information). It is likely that the increased reverse bias improves electron transport toward the ZnO contact. Alternatively, the EQE above 100% can be related to trapped charge carriers, facilitating tunneling transport of the opposite carrier. This phenomenon has been studied by Li et al., reporting the photomultiplication in poly(3-hexylthiophene) (P3HT) doped with ≤15 wt% PC$_{71}$BM.[38] Due to the absence of electron transport channels, electrons on isolated fullerene domains are trapped and create an electric field in the device. The resulting band bending facilitates hole tunneling injection current, causing an EQE > 100%. Possibly, in the bilayer–ternary devices, trapped electrons at the interface result in enhanced hole tunneling injection current from the holes generated in the PDCB-2T layer via PDPP2T-TT toward the MoO$_3$/Ag contact. Illuminating the PDPP2T-TT:PC$_{61}$BM blend with 730 nm bias light could facilitate electron trapping, causing an EQE > 100% when holes are generated in the PDCB-2T material upon illumination with 530 nm probe light. Reduction of the EQE overshoot with additional 530 nm bias illumination (Figure 7a) and the application of a reverse bias (Figure 7b) may be related to a reduced density of trapped electrons. However, no evidence can be provided for this tentative explanation.

Hampered electron transport in bilayer–ternary devices was confirmed by analyzing hole-only and electron-only devices in the dark (**Table 4**). PDPP2T-TT:PC$_{61}$BM active layers fabricated by spin coating and spontaneous spreading show high hole mobilities (μ_h). A similar mobility was measured for bilayer–ternary devices, indicating that the photogenerated holes do not experience an extraction barrier. This agrees with the high FF

of 0.65 observed in J–V characteristics measured for a ternary device illuminated by 530 nm monochromatic light (Figure 5a). Under these conditions, the holes generated in the PDCB-2T:PC$_{61}$BM layer cross the interface without losses. In contrast, electrons injected into bilayer–ternary devices do not reach the space-charge limit. The double logarithmic J–V plot in Section S8 and Figure S9c (Supporting Information) show a slope significantly higher than 2 for electron transport in bilayer devices. This indicates that the electron current is trap-limited or that the injection of electrons in the PDPP2T-TT:PC$_{61}$BM layer is not Ohmic due to the formation of a barrier caused by the built-up of electrons at the interface.[39,40] A high slope in the log$J$–log$V$ plot was also measured for bilayer PDPP2T-TT:PC$_{61}$BM solar cells, even though they exhibit good J–V characteristics. For these devices, no overshoot in EQE can be measured because the two sublayers cannot be probed separately. A possible negative influence of water on the charge transport properties of the PDPP2T-TT:PC$_{61}$BM layer can be excluded as Table 4 shows good electron and hole mobility for a PDPP single layer device made by spontaneous spreading.

A possible barrier for electron transport over the interface may be the result of the different surface tension of the donor and acceptor materials, causing the layer/air or layer/water interfaces to be enriched with one of the compounds. X-ray photoelectron spectroscopy (XPS) in combination with ion beam sputtering (Section S9, Supporting Information), however, did not reveal any concentration gradient for both the spin-coated PDCB-2T:PC$_{61}$BM films and for SVA PDPP2T-TT:PC$_{61}$BM bilayer fabricated by spontaneous spreading. With XPS depth profiling, the interface between the two PDPP2T-TT:PC$_{61}$BM layers cannot be distinguished from the bulk signal. It can be concluded that concentration gradients in the active layers of the ternary device are not significant and cannot be the reason for an energy barrier. We note that XPS depth profiling on the bilayer–ternary blend did reveal clear concentration steps for sulfur and nitrogen (Figure S10c, Supporting Information).

Additional proof that concentration gradients or surface enrichment in the PDPP2T-TT:PC$_{61}$BM are not likely to cause the EQE > 100% was found by the fabricating bilayer–ternary devices, by both stamping and scooping the PDPP2T-TT:PC$_{61}$BM layer from the water substrate. In this way, bilayer–ternary devices have been made in which the surface of the PDPP2T-TT:PC$_{61}$BM layer was in contact with either the air or water interface before contacting with the PDCB-2T:PC$_{61}$BM layer. Both the bilayer–ternary cells showed similar performance and overshoots in the EQE. Details are presented in Section S10 (Supporting Information).

Further confirmation that hampered electron transport is related to the interface between the two sublayers in the ternary device obtained by comparing the device performance of the bilayer–ternary device to a single layer ternary solar cell. The single layer device was fabricated by mixing PDCB-2T, PDPP2T-TT, and PC$_{61}$BM in a 1:1:3 ratio dissolved in chloroform with 5 vol% DIO. After spin coating this solution, the layer was treated with solvent vapor, as has been

Table 4. Hole- and electron-mobility data obtained from J–V data fitted with the Mott–Gurney law for space charge limited current (SCLC).

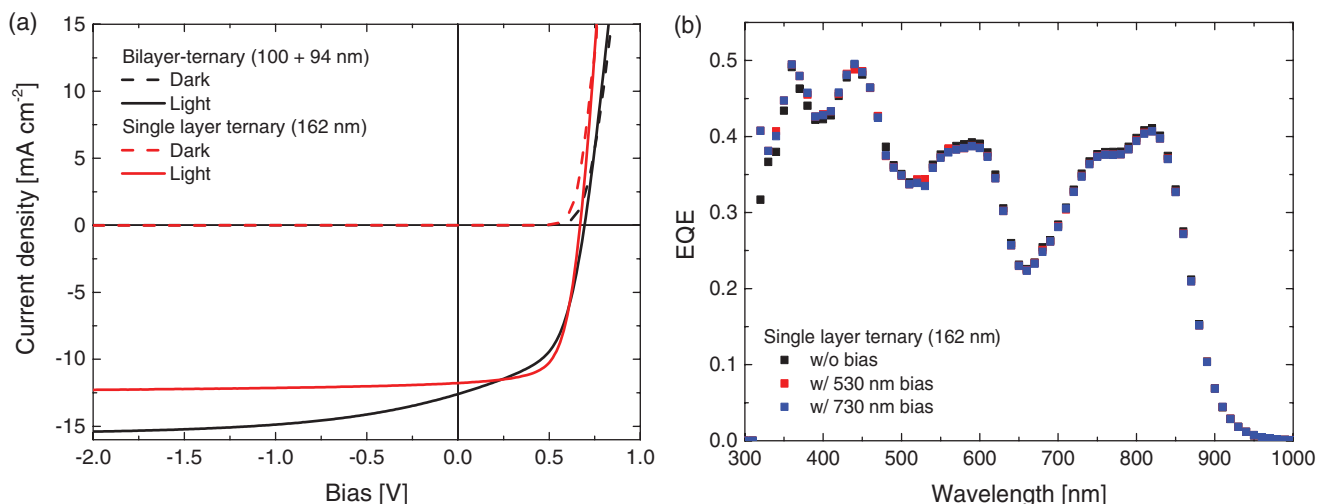| Device	Deposition	μ_h [cm^2 V^{-1} s^{-1}]	μ_e [cm^2 V^{-1} s^{-1}]
PDCB-2T:PC$_{61}$BM	SC	$(2.9 \pm 1.3) \times 10^{-5}$	$(3.1 \pm 1.5) \times 10^{-5}$
PDPP2T-TT:PC$_{61}$BM	SC	$(2.4 \pm 1.1) \times 10^{-4}$	$(7.7 \pm 4.0) \times 10^{-6}$
Single layer PDPP2T-TT:PC$_{61}$BM	SS	Shorted	$(2.4 \pm 1.3) \times 10^{-5}$
Bilayer PDPP2T-TT:PC$_{61}$BM	SS | SS	$(1.6 \pm 0.3) \times 10^{-4}$	No SCLC
Bilayer–ternary	SC | SS	$(1.2 \pm 0.2) \times 10^{-4}$	No SCLC

Figure 8. a) J–V characteristics of a single layer ternary device with an active layer thickness of 162 nm. $J_{SC} = 11.8$ mA cm^{-2}, $V_{OC} = 0.67$ V, FF = 0.65, $P_{max} = 5.1$ mW cm^{-2} with simulated AM1.5G illumination. b) EQE measured without and with 530 or 730 nm bias light. $J_{SC}^{EQE} = 11.7$ mA cm^{-2} (w/o bias light), PCE = 5.1%.

done for the bilayer–ternary devices. The results are shown in **Figure 8**. Although a comparable performance of 5.1% has been achieved, the J–V and EQE characteristics of the single layer ternary device are markedly different than the bilayer–ternary device. Illuminating the single layer device with LED sources of high and low wavelength does not change the EQE due to the homogeneous charge density throughout the active layer. Additionally, the single layer device shows significantly higher FF compared to the bilayer architecture which may be a limit for the performance of bilayer–ternary devices. We conclude that the hampered electron transport observed for the bilayer–ternary device is caused by the interface created between the two sublayers.

To avoid electron transport from the PDPP2T-TT:PC$_{61}$BM layer over the interface with PDCB-2T:PC$_{61}$BM, bilayer–ternary devices have been made in a regular device configuration depicted in **Figure 9** and the device characteristics are summarized in **Figure 10** and **Table 5**. Compared to an inverted configuration bilayer–ternary solar cell with similar active layer
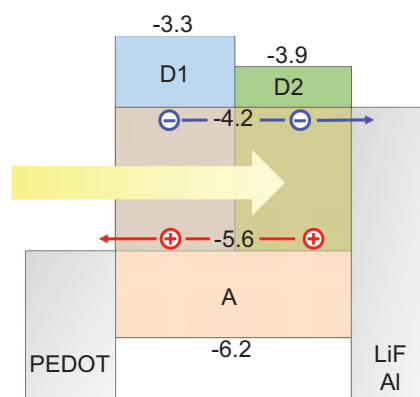

Figure 9. Regular device architecture including the energy levels of the layers.

thicknesses, the device in the regular configuration displays a low FF. This is the result of a bias-dependent charge extraction around J_{SC}, which is also present under illumination with 530 and 730 nm light (Figure 10). When illuminating the device with 530 nm light, the extraction efficiency of the carriers is worse, which is related to a decreased EQE under 530 nm light bias compared to the measurement without bias. Although the configuration of the device is altered, the effect of bias illumination on the electric field within the device is expected to be the same, as has been calculated for the inverted device (Figure 6 and Section S6 (Supporting Information)). However, with the addition of bias light, no EQE enhancement has been measured for most of the devices. In an exceptional case, an EQE improvement of 37% was measured for which the data are presented in Section S11 (Supporting Information). The absence of overshoots in EQE above 100% evidences that there is no charge accumulation in the regular devices caused by a barrier for charge extraction. These results confirm our hypothesis that the overshoot measured with 730 nm bias light in inverted configurations is related to hampered electron transport over the interface between the two photoactive layers, as this is avoided in regular configuration devices.

The results discussed above raise the question whether the hampered electron transport and EQE overshoot are intrinsic properties of the bilayer architecture or if they are caused by the specific material combination. Therefore, a device was made with poly[N-9′-heptadecanyl-2,7-carbazole-alt-5,5-(4′,7′-di-2-thienyl-2′,1′,3′-benzothiadiazole)] (PCDTBT) as the donor polymer together with PC$_{61}$BM in the first layer of a bilayer–ternary device. The results are summarized in Section S12 (Supporting Information) and show that similar to the results of the PDCB-2T:PC$_{61}$BM/PDPP2T-TT:PC$_{61}$BM ternary devices, the EQE of the PDPP2T-TT:PC$_{61}$BM layer decreases upon 730 nm bias illumination. Although enhanced EQEs can be measured in the low wavelength regime for PCDTBT:PC$_{61}$BM/PDPP2T-TT:PC$_{61}$BM bilayer–ternary devices, an EQE > 100% has not been measured. The similar behavior in EQE of the two ternary

ADVANCED
SCIENCE NEWS
www.advancedsciencenews.com

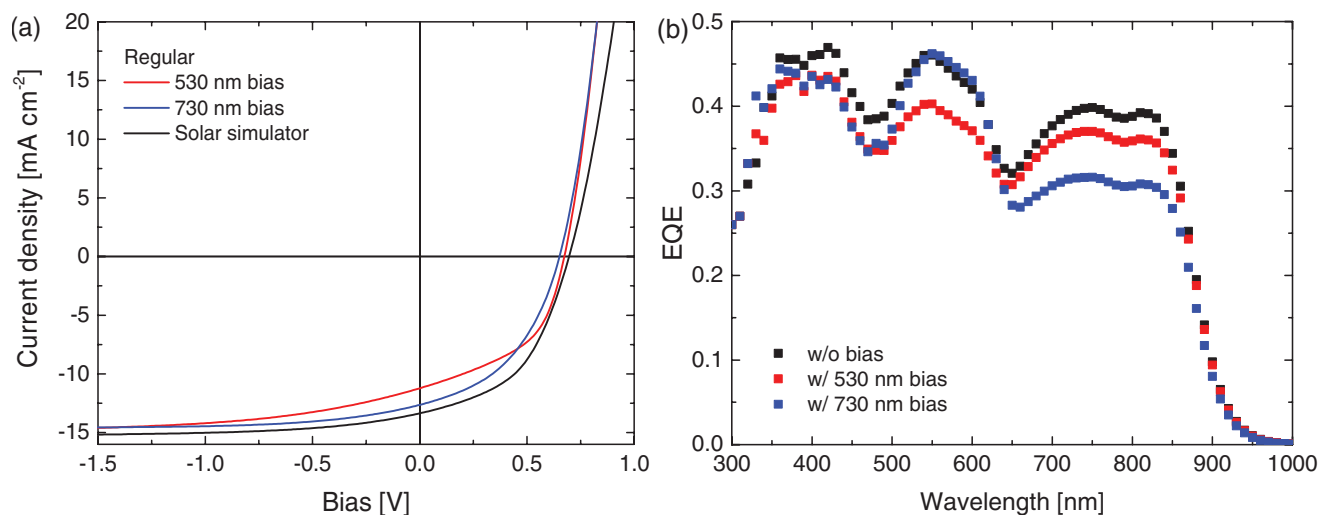ADVANCED
ENERGY
MATERIALS
www.advenergymat.de

Figure 10. a) J–V characteristics of a bilayer–ternary device in a regular configuration illuminated with different light sources. The bilayer consists of a 133 nm PDCB-2T:PC$_{61}$BM bottom layer and 123 nm PDPP2T-TT:PC$_{61}$BM top layer. b) EQE measured without and with 530 or 730 nm bias light. $J_{SC}^{EQE} = 12.96$ mA cm^{-2} (w/o bias light).

devices hints that hampered electron transport over the interface in the ternary architecture is not necessarily related to the specific material combination. Besides changing the wide bandgap polymer in the first layer of the ternary device, effects of the high DIO content in the PDPP2T-TT:PC$_{61}$BM solution on the underlying layer has been investigated. Possibly, DIO can partly dissolve the fullerene in the PDCB-2T:PC$_{61}$BM active layer, altering the surface morphology of the blend. Therefore, a bilayer–ternary device has been fabricated in which the PDPP2T-TT active layer is processed by spontaneous spreading from a CB/1,2-dichlorobenzene (o-DCB) solution. The results of this device stack are summarized in Section S13 (Supporting Information) and do not show a significant reduction in the EQE overshoot when illuminating the device with 730 nm bias light. It can be concluded that DIO does not influence the PDCB-2T active layer such that a barrier for charge transport is created.

3. Conclusion

The spontaneous spreading technique on an aqueous surface is an interesting method for the fabrication of polymer–fullerene bulk-heterojunction layers for organic solar cells. For PDPP2T-TT:PC$_{61}$BM cells, we have shown that the photovoltaic performance of layers deposited by spontaneous spreading is comparable to that of spin-coated layers. The morphologies of the photoactive layers consist of fibrous polymer networks, as was established by TEM for both the methods. At similar layer

thickness, PDPP2T-TT:PC$_{61}$BM layers deposited by spontaneous spreading provide somewhat higher short-circuit current, but a lower fill factor than that of spin-coated layers, consistent with a somewhat coarser morphology for spin-coated layers.

Spontaneous spreading also enables the fabrication of bilayer ternary devices in which two different bulk heterojunctions can be placed on top of each other. This was demonstrated by combining a wide bandgap PDCB-2T:PC$_{61}$BM front layer and a small bandgap PDPP2T-TT:PC$_{61}$BM back layer in an inverted bilayer–ternary blend cell. The power conversion efficiency of this novel bilayer–ternary solar cell configuration exceeds that of the corresponding single layer devices. The bilayer–ternary solar cells exhibit extraordinary device characteristics. Selective illumination of the back layer with light of 730 nm reveals a lower FF in the J–V characteristics than with simulated AM1.5G illumination, as a result of hampered transport of electrons across the interface of the two bulk heterojunction layers. We consider that electrons generated in the PDPP2T-TT:PC$_{61}$BM back layer accumulate at the interface as a consequence of a barrier for electron transport. Interestingly, this barrier can be reduced when the carrier density in the PDCB-2T:PC$_{61}$BM layer front layer is increased by illuminating with a low intensity probe light of 530 nm. Hence, under 730 nm bias illumination, the EQE at 530 nm can be more than doubled to values exceeding 100%. Under these conditions, charges generated in the back layer by 730 nm light are more efficiently collected when simultaneously illuminating the front layer. Likewise, an EQE enhancement of 30% has been observed in the high wavelength regime when the front layer is biased with 530 nm light.

Table 5. Device characteristics determined by J–V measurements of a regular versus inverted bilayer–ternary device.

Device	d_{PDCB} [nm]	d_{PDPP} [nm]	J_{SC} [mA cm^{-2}][a]	V_{OC} [V][a]	FF[a]	P_{max} [mW cm^{-2}][a]
Inverted	133	123	11.8 (10.7 ± 1.03)	0.70 (0.69 ± 0.01)	0.56 (0.56 ± 0.01)	4.6 (4.1 ± 0.44)
Regular	104	142	13.4 (12.8 ± 0.43)	0.70 (0.69 ± 0.00)	0.48 (0.48 ± 0.00)	4.5 (4.3 ± 0.14)

[a]Performance of the best device obtained from J–V measurements and between brackets, the average result ± standard deviation of 4 devices.

Drift-diffusion calculations show that carrier generation and the electric field distribution are inhomogeneous when selectively exciting front or back layers at high intensity. This causes wavelength- and intensity-dependent splitting of the quasi-Fermi energy levels which can lead to a significant (>20%) enhancement of the EQE. Hence, the drift-diffusion simulations confirm the EQE enhancement, but are not able to account for the magnitude of the effect. Experimental results indicate that the additional increase is related to a barrier for electron transport at the interface of the two sublayers. Despite suboptimal charge transport, good device performance up to PCE = 5.9% has been achieved for bilayer–ternary devices under simulated AM1.5 conditions. This demonstrates that spontaneous spreading on aqueous surfaces is an interesting method to fabricate unconventional device architectures with good performance.

4. Experimental Section

Device Fabrication: Photovoltaic devices were made by spin coating a ZnO sol–gel layer on cleaned, patterned ITO substrates in air (14 Ω □⁻¹) (Naranjo Substrates). The ZnO sol–gel was prepared by dissolving Zn(OAc)$_2$ (Sigma-Aldrich) (109.6 mg) in 2-methoxyethanol (Sigma-Aldrich) (1 mL), and adding ethanolamine (Sigma-Aldrich) (30.2 µL). This mixture was stirred at room temperature for at least 1 h. The resulting sol–gel was spin-coated at 4000 rpm and annealed for 5 min at 150 °C under ambient conditions. For spontaneous spreading, PDPP2T-TT (synthesized according to ref. [34]) and PC$_{61}$BM (Solenne BV) were dissolved in a 1:3 weight ratio in chlorobenzene containing 10 vol% DIO (Alfa Aesar). The total concentration of the solution was 35 mg mL⁻¹. The optimization of the solvent mixture is discussed in the Supporting Information. This mixture was stirred for at least 4 h at 140 °C and overnight at 90 °C. Before spreading, it was cooled down for 1 h at room temperature. Layers for solar cell fabrication were made by dropping 20 µL of this solution on a Petri dish of 9 cm in diameter filled with water. When the chlorobenzene had evaporated (after ≈20 s), the layer could be transferred. PDPP2T-TT:PC$_{61}$BM devices fabricated by spin coating were made from a 1:3 w/w solution of the respective compounds in chloroform to which 7.5 vol% o-dichlorobenzene was added. This solution had a total concentration of 16 mg mL⁻¹. For the fabrication of ≈100 nm thick PDCB-2T:PC$_{61}$BM layers, the donor (synthesized according to ref. [35]) and acceptor were dissolved in a 1:1.5 weight ratio in chloroform to which 2 vol% diphenyl ether was added to a total concentration of 15 mg mL⁻¹. To ensure complete dissolution, the mixture was stirred at 90 °C for at least 1.5 h and after cooling down to room temperature, it was spin-coated at 1300 rpm under ambient conditions. Inverted devices were completed by evaporating MoO$_3$ (10 nm) and Ag (100 nm) as top electrode under a vacuum of ≈3 × 10⁻⁷ mbar, while regular configuration devices had a LiF (1 nm) and Al (100 nm) top contact. The active area of the cells was 0.09 or 0.16 cm².

Absorption Spectroscopy: Optical absorption spectra were measured with a PekinElmer Lambda 1050 UV/vis/NIR spectrophotometer.

Device Characterization: Current density–voltage (J–V) characteristics were measured under simulated AM1.5G solar light of 100 mW cm⁻². This was achieved by a Hoya LB100 daylight filter that was placed in between the solar cell and a tungsten–halogen lamp. To perform a J–V sweep, a Keithley 2400 sourcemeter was used. All measurements were conducted in nitrogen-filled glove box. Device performances were quoted as maximum power (P_{max}) (mW cm⁻²) when the short-circuit current density (J_{SC}) was obtained from the J–V curve measured under simulated solar light of 100 mW cm⁻², and as PCE (%) when J_{SC} was determined more accurately from the EQE by integrating the spectra with AM1.5G solar spectrum. EQE measurements were performed in a homebuilt setup, which consisted of a 50 W tungsten halogen lamp (Osram 64610),

a mechanical chopper (Stanford Research, SR 540), a monochromator (Oriel, Cornerstone 130) and finally, the device kept in a nitrogen-filled box with a quartz window which was illuminated through an aperture of 2 mm. This measurement was also performed in combination with a continuous LED bias light with a wavelength of 730 or 530 nm (Thor Labs). The current of this bias light could be adjusted such that an illumination intensity equal to AM1.5G was reached. The response was recorded using a low noise current preamplifier (Stanford Research System SR 570) and lock-in amplifier (Stanford Research Systems SR 830). For light intensity–dependent current measurements, the generated current of the device was measured by a Keithley 2400 with increasing intensity of the 530 or 730 nm LED.

Transmission Electron Microscopy: TEM samples of layers prepared by spontaneous spreading were prepared by scooping the active layer floating on water on to a 200 square mesh copper grid. TEM samples of active layers prepared in the inverted device stack were prepared by floating of the active layer from a ZnO sol–gel layer. The ZnO layer was dissolved in acidified water after which the active layer was transferred to a grid. For analyzing the layers, a Tecnai G2 Sphera was used with a voltage of 200 kV at a magnification range of 1150× to 80 000× and the corresponding defocus values of −10 µm and −400 nm, respectively. To avoid beam damage to the sample, the beam was blocked in low-dose mode while moving to another position at the sample.

Device Simulation: Drift-diffusion calculations were performed on bilayer–ternary devices having a thickness of 70 nm for the PDCB-2T:PC$_{61}$BM layer with a 100 nm PDPP-2T-TT:PC$_{61}$BM blend on top. A carrier mobility of 1 × 10⁻⁴ cm² V⁻¹ s⁻¹ was used and for simplicity, it was assumed that the mobility of holes and electrons was balanced and similar in both active layers. In the simulation, bimolecular (Langevin) recombination was assumed with prefactor γ_{pre} = 0.01. An energetic offset of 0.2 eV was set between the HOMO energy levels of PDCB-2T and PDPP-2T-TT. Injection barriers for electrons and holes into the blend were set at 0.2 eV. The quasi-Fermi level potentials $\phi_{n(p)}$ were calculated according to $\phi_n = \psi - (kT/q)\ln(n/n_i)$ and $\phi_p = \psi + (kT/q)\ln(p/n_i)$ with ψ the potential across the device, n_i the intrinsic carrier concentration, k the Boltzmann constant, q the elementary charge, and T the temperature. The quasi-Fermi level potentials were calculated under different illumination conditions with probe light having a photon flux of ≈10¹⁵ cm⁻² s⁻¹ and bias light having a photon flux of ≈10¹⁷ cm⁻² s⁻¹. To reflect to 100-fold difference in photon flux, the electron–hole pair generation rate was set to G = 10²⁶ m⁻³ s⁻¹ for low intensity probe light and to G = 10²⁸ m⁻³ s⁻¹ for bias illumination, respectively.

Charge Mobility: Mobility measurements were performed on hole-only and electron-only devices. For hole-only devices, the active layer was deposited on a substrate coated with poly(ethylenedioxythiophene)-:poly(styrenesulfonate) (PEDOT:PSS) and finished with a MoO$_3$/Ag top contact, while for electron-only devices, ZnO and LiF/Al were used as contact materials. The current versus voltage measurements were performed in the dark up to a voltage of 8 V. Plotting the results on a log–log scale revealed in which voltage range the J_{SC} was space-charge limited. For this voltage range, the mobility was determined by fitting the dark J–V curves to the Mott–Gurney law.

Supporting Information

Supporting Information is available from the Wiley Online Library or from the author.

Acknowledgements

1802197 (11 of 12)

Conflict of Interest

The authors declare no conflict of interest.

Keywords

bilayer–ternary solar cells, polymer solar cells, sequential deposition, spontaneous spreading

[1] M. C. Scharber, N. S. Sariciftci, *Prog. Polym. Sci.* **2013**, *38*, 1929.
[2] R. Søndergaard, M. Hösel, D. Angmo, T. T. Larsen-Olsen, F. C. Krebs, *Mater. Today* **2012**, *15*, 36.
[3] Y. Liu, J. Zhao, Z. Li, C. Mu, W. Ma, H. Hu, K. Jiang, H. Lin, H. Ade, H. Yan, *Nat. Commun.* **2014**, *5*, 6293.
[4] W. Li, J. Cai, F. Cai, Y. Yan, H. Yi, R. S. Gurney, D. Liu, *Nano Energy* **2018**, *44*, 155.
[5] Q. Wan, X. Guo, Z. Wang, W. Li, B. Guo, W. Ma, M. Zhang, Y. Li, *Adv. Funct. Mater.* **2016**, *26*, 6635.
[6] Z. Li, D. Yang, X. Zhao, T. Zhang, J. Zhang, X. Yang, *Adv. Funct. Mater.* **2018**, *28*, 1705257.
[7] S. Li, W. Liu, C. Li, M. Shi, H. Chen, *Small* **2017**, *13*, 1701120.
[8] F. Zhao, S. Dai, Y. Wu, Q. Zhang, J. Wang, L. Jiang, *Adv. Mater.* **2017**, *29*, 1700144.
[9] H. Bin, L. Gao, Z. Zhang, Y. Yang, Y. Zhang, C. Zhang, S. Chen, L. Xue, C. Yang, M. Xiao, Y. Li, *Nat. Commun.* **2016**, *7*, 13651.
[10] C. Sun, F. Pan, H. Bin, J. Zhang, L. Xue, B. Qiu, Z. Wei, Z. Zhang, Y. Li, *Nat. Commun.* **2018**, *9*, 1.
[11] W. Zhao, S. Li, H. Yao, S. Zhang, Y. Zhang, B. Yang, J. Hou, W. Zhao, S. Li, H. Yao, S. Zhang, Y. Zhang, B. Yang, *J. Am. Chem. Soc.* **2017**, *139*, 7148.
[12] Z. Fei, F. D. Eisner, X. Jiao, M. Azzouzi, J. A. Röhr, Y. Han, M. Shahid, A. S. R. Chesman, C. D. Easton, C. R. Mcneill, T. D. Anthopoulos, J. Nelson, M. Heeney, *Adv. Mater.* **2018**, *30*, 1705209.
[13] X. Xu, T. Yu, Z. Bi, W. Ma, Y. Li, Q. Peng, *Adv. Mater.* **2018**, *30*, 1703973.
[14] S. Zhang, Y. Qin, J. Zhu, J. Hou, *Adv. Mater.* **2018**, *1800868*, 1.
[15] A. D. De Zerio, C. Müller, *Adv. Energy Mater.* **2018**, *8*, 1702741.
[16] Y. Chen, Y. Qin, Y. Wu, C. Li, H. Yao, N. Liang, X. Wang, *Adv. Energy Mater.* **2017**, *7*, 1700328.
[17] C. Lindqvist, J. Bergqvist, O. Bäcke, S. Gustafsson, E. Wang, E. Olsson, O. Inganäs, M. R. Andersson, C. Müller, *Appl. Phys. Lett.* **2014**, *104*, 153301.
[18] N. Gasparini, X. Jiao, T. Heumueller, D. Baran, G. J. Matt, S. Fladischer, E. Spiecker, H. Ade, C. J. Brabec, *Nat. Energy* **2016**, *1*, 16118.
[19] W. Huang, P. Cheng, Y. M. Yang, G. Li, Y. Yang, *Adv. Mater.* **2018**, *30*, 1705706.
[20] X. Ma, Y. Mi, F. Zhang, Q. An, M. Zhang, Z. Hu, *Adv. Energy Mater.* **2018**, *8*, 1702854.
[21] Z. Xiao, X. Jia, L. Ding, *Sci. Bull.* **2017**, *62*, 1562.
[22] T. Kumari, S. M. Lee, S.-H. Kang, S. Chen, C. Yang, *Energy Environ. Sci.* **2017**, *10*, 285.
[23] N. Felekidis, A. Melianas, M. Kemerink, *ACS Appl. Mater. Interfaces* **2017**, *9*, 37070.
[24] Q. Ai, W. Zhou, L. Zhang, L. Huang, J. Yin, Z. Yu, S. Liu, W. Ma, J. Zeng, Y. Chen, *J. Mater. Chem. C* **2017**, *5*, 10801.
[25] L. Lu, W. Chen, T. Xu, L. Yu, *Nat. Commun.* **2015**, *6*, 7327.
[26] J. Zhang, Y. Zhao, J. Fang, L. Yuan, B. Xia, G. Wang, *Small* **2017**, *13*, 1700388.
[27] H. Huang, L. Yang, B. Sharma, *J. Mater. Chem. A* **2017**, *5*, 11501.
[28] M. Ghasemi, L. Ye, Q. Zhang, L. Yan, J.-H. Kim, O. Awartani, W. You, A. Gadisa, H. Ade, *Adv. Mater.* **2017**, *29*, 1604603.
[29] J. Huang, H. Wang, K. Yan, X. Zhang, H. Chen, *Adv. Mater.* **2017**, *29*, 1606729.
[30] J. K. Kim, W. Kim, D. H. Wang, H. Lee, S. M. Cho, D. Choi, J. H. Park, *Langmuir* **2013**, *29*, 5377.
[31] J. Noh, S. Jeong, J.-Y. Lee, *Nat. Commun.* **2016**, *7*, 12374.
[32] A. H. Demond, A. S. Lindner, *Environ. Sci. Technol.* **1993**, *27*, 2318.
[33] Q. Wang, F. Yang, Y. Zhang, M. Chen, Q. Wang, F. Yang, Y. Zhang, M. Chen, X. Zhang, *J. Am. Chem. Soc.* **2018**, *140*, 5339.
[34] W. Li, K. H. Hendriks, W. S. C. Roelofs, Y. Kim, M. M. Wienk, R. A. J. Janssen, *Adv. Mater.* **2013**, *25*, 3182.
[35] R. Heuvel, F. J. M. Colberts, M. M. Wienk, R. A. J. Janssen, *J. Mater. Chem. C* **2017**, *25*, 3182.
[36] L. J. A. Koster, M. Kemerink, M. M. Wienk, K. Maturová, R. A. J. Janssen, *Adv. Mater.* **2011**, *23*, 1670.
[37] H. Choi, S. Ko, T. Kim, P. Morin, B. Walker, B. H. Lee, M. Leclerc, J. Y. Kim, A. J. Heeger, *Adv. Mater.* **2015**, *27*, 3318.
[38] L. Li, F. Zhang, J. Wang, Q. An, Q. Sun, W. Wang, J. Zhang, F. Teng, *Sci. Rep.* **2015**, *5*, 9181.
[39] P. Mark, W. Helfrich, P. Markt, *J. Appl. Phys.* **1962**, *33*, 205.
[40] M. A. Lampert, *Phys. Rev.* **1956**, *103*, 1648.